Spin density in YTiO₃: I. Joint refinement of polarized neutron diffraction and magnetic x-ray diffraction data leading to insights into orbital ordering

I. A. Kibalin,[1,2,4] Z. Yan,[3] A. B. Voufack,[4] S. Gueddida,[3] B. Gillon,[1,*] A. Gukasov,[1] F. Porcher,[1] A. M. Bataille,[1]
F. Morini,[4] N. Claiser,[4] M. Souhassou,[4] C. Lecomte,[4] J.-M. Gillet,[3] M. Ito,[5] K. Suzuki,[5] H. Sakurai,[5]
Y. Sakurai,[6] C. M. Hoffmann,[7] and X. P. Wang[7]

[1]*Laboratoire Léon Brillouin, CEA, Centre National de la Recherche Scientifique, CE-Saclay, 91191 Gif-sur-Yvette, France*
[2]*PNP NRC "Kurchatov Institute" Orlova Rosha, Gatchina, 188300 Leningrad Region, Russia*
[3]*Laboratoire SPMS, UMR 8580, Centrale Supélec, 92295 Chatenay-Malabry, France*
[4]*CRM2, Institut Jean Barriol, University of Lorraine and Centre National de la Recherche Scientifique,
Vandoeuvre-les-Nancy, BP239, F54506, France*
[5]*Graduate School of Science and Technology, Gunma University, 1-5-1 Tenjin-cho, Kiryu, Gunma 376-8515, Japan*
[6]*Japan Synchrotron Radiation Research Institute, SPring-8,1-1-1 Kouto, Sayo, Hyogo 679-5198, Japan*
[7]*Chemical and Engineering Materials Division, Oak Ridge National Laboratory, 1 Bethel Valley Road, Oak Ridge, Tennessee 37831, USA*

Orbital ordering below 30 K was previously observed in the ferromagnetic YTiO₃ compound both by polarized neutron diffraction (PND) and x-ray magnetic diffraction (XMD). In this paper we report a procedure for the joint refinement of a unique spin-density model based on both PND and XMD data. The distribution of the unpaired $3d$ electron of titanium is clearly seen on the magnetization density reconstructed by the maximum entropy method from the PND data collection at 5 K. The Ti³⁺ $3d$ orbital populations obtained by joint model refinement are discussed in terms of the orbital ordering scheme. Small but significant magnetic moments on apical oxygen O₁ and yttrium atoms are found. The agreement between experimental and theoretical spin densities obtained using density functional theory is discussed.

I. INTRODUCTION

Among the titanates presenting a pseudocubic perovskite structure and showing an orbital ordering phenomenon, the perovskite-type YTiO₃ crystal has drawn considerable attention because of the existence of antiferromagnetic orbital ordering in the ferromagnetic state. YTiO₃ is a ferromagnetic insulator with a Curie temperature of 30 K. It has been investigated theoretically [1–3] and by various experimental techniques such as nuclear magnetic resonance [4], polarized and unpolarized neutron diffraction [5,6], inelastic neutron scattering [7], resonant x-ray scattering [8], soft x-ray linear dichroism [9], x-ray magnetic diffraction [10], Compton scattering [11], and elastic x-ray scattering [12]. Theoretical studies using unrestricted Hartree-Fock calculation and density functional theory (DFT) with generalized gradient approximation predicted the wave functions of the orbital ordering state of the $3d$ electrons of Ti atoms to be the linear combination of $|yz\rangle$ and $|xz\rangle$ orbitals of the t_{2g} state [1].

The first direct evidence of orbital ordering in YTiO₃ has been given by Akimitsu *et al.* [6] by using the polarized neutron-diffraction (PND) technique. Experimental magnetic form factors of "special" reflections originating from the aspherical contribution of the Ti spin density were measured. It was noted that these magnetic reflections are forbidden in the spherical approximation for magnetic structure factor calculations. An appearance of magnetic response at these reciprocal points is directly related to the existence of the orbital ordering. Moreover, the measured magnetic form factors were confronted with a model of orbital ordered

configuration of the t_{2g} electrons matching the symmetry of the Jahn-Teller distortion. It was found that the populations of the $|yz\rangle$ and $|xz\rangle$ orbitals in the t_{2g} state orbital functions, fitted from experimental results, are in agreement with the model [6].

The "antiferromagnetic" orbital ordering in YTiO₃ was also confirmed by x-ray magnetic diffraction (XMD) experiments [10,13]. The magnetic form factor obtained for a total of 62 reciprocal-lattice points was found in agreement with the calculated one using the ordered orbital model mentioned above. Moreover, the XMD technique allowing the separation of orbital (L) and spin (S) form factors gave evidence for the total quenching of the orbital moment in YTiO₃ [10]. We note that PND and XMD methods are rather complementary: PND typically provides information on the magnetic form factor for scattering vectors with $\sin(\theta)/\lambda < 0.6\,\text{Å}^{-1}$, thus giving information about the outer part of the spin distribution, while the XMD operating at $\sin(\theta)/\lambda > 0.3\,\text{Å}^{-1}$ is more sensitive to its inner part. Thus, a joint refinement of the PND and the XMD data may give insight on the spin distribution and, hence, orbital ordering in YTiO₃.

Unfortunately, the PND data set reported in [6] is quite limited as it contains only zonal reflections ([0kl], [h0l], and [hk0]). Recent progress in polarized neutron-diffraction technique due to the use of area detectors [14] and more efficient polarizers [15] as installed at LLB-Orphée (Saclay) allows fast acquisition of flipping ratios in a large portion of the reciprocal space. Therefore a series of flipping ratio measurements has been undertaken on YTiO₃ with the aim to achieve the highest possible data completeness and redundancy with a $0.6\,\text{Å}^{-1}$ resolution. High completeness was found to be very important not only in the model refinement but in particular when using a model-free analysis of data based on the reconstruction of the three-dimensional spin distribution by the maximum entropy

———————
*beatrice.gillon@cea.fr

method (MEM). We used MEM reconstruction to uncover the presence of spin density on the ligands. Here we present the results of these PND studies on YTiO$_3$ and the results of their joint treatment with XMD data.

This paper is part of a larger project which aims at developing a model of the experimental spin-resolved electron density common to experimental techniques as different as high-resolution x-ray diffraction (XRD), PND, XMD, and magnetic inelastic Compton scattering (M-ICS). Previous work has shown that spin-resolved electron density can be modeled using joint refinement against x-ray-diffraction, neutron-diffraction, and polarized-neutron-diffraction data [16]. While PND gives access to the spin density in the position space, M-ICS permits one to explore spin density in momentum space. The results thus obtained by M-ICS for YTiO$_3$ will be presented in Ref. [17] and compared to the present spin density in position space.

II. EXPERIMENTAL

A. Unpolarized neutron diffraction

A single crystal of YTiO$_3$ of size $(1 \times 2 \times 3.5)$ mm^3 was used in all experiments. The crystal was provided by one of the authors. Prior to spin-density studies, the nuclear structure was investigated at the hot neutron four-circle diffractometer 5C2 (LLB-Orphée, Saclay) using $\lambda = 0.84$ Å. A total of 850 reflections up to $\sin\theta/\lambda = 0.60$ Å^{-1} were measured and 280 unique ones $(218 > 3\sigma)$ were obtained by merging equivalents, using space group $Pnma$. In order to reveal possible deviations from the $Pnma$ symmetry in the ferromagnetic phase, data collections were performed at room temperature, in the paramagnetic phase at $T = 40$ K (above the Curie temperature $T_C = 30$ K) and in the ferromagnetic phase at $T = 14$ K. Since numerous reflections violating $Pnma$ special extinction rules were observed in these data sets, an *ab initio* structure determination was carried out on the single crystal diffractometer TOPAZ (Spallation Neutron Source, Oak Ridge) at $T = 90$ K and room temperature. At each temperature more than 5500 reflections (up to $\sin\theta/\lambda = 1.00$ Å^{-1}) were measured. Details on the TOPAZ data collection are provided in Table 1S of Ref. [18].

B. PND

Magnetization density studies were performed at the thermal polarized neutron lifting counter diffractometer 6T2 (LLB-Orphée, Saclay) [15]. Neutrons of wavelength 1.4 Å were monochromated by vertically focusing graphite crystal and polarized by a supermirror bender. The polarization factor of the beam was $p = 0.95$. In order to fully magnetize the sample, a 5-T magnetic field was applied. Data were collected at three different sample orientations, along the main crystallographic axes a, b, and c, respectively, oriented parallel to magnetic field. Flipping ratios R_{PND} [Eq. (1)], i.e., the ratios between the spin-up and spin-down intensities of more than 260 (hkl) reflections, were measured in the ferromagnetic phase at 5 K:

$$R_{\text{PND}} = \frac{y^+}{y^-} \times \frac{F_N^2 + 2pq^2 F_N F_M + q^2 F_M^2}{F_N^2 - 2peq^2 F_N F_M + q^2 F_M^2}. \quad (1)$$

F_M and F_N denote the magnetic and nuclear structure factors. $q = \sin\alpha$ is a geometric factor with α being the angle between the scattering and the magnetization vector. e is the flipping efficiency. The parameters $y^\pm$ are extinction coefficients [see Eq. (4)].

Additional measurements with polarized neutrons have been carried out on the hot neutron spin-polarized two axis diffractometer 5C1 (LLB-Orphée, Saclay). Neutrons from the source are monochromated and polarized by the (111) reflection of a magnetized Heusler crystal Cu$_2$MnAl. The wavelength is 0.84 Å, which corresponds to the maximum flux of the hot source and it is ideal for studying large domains of reciprocal space. The polarization factor of the beam is $p = 0.90$. A magnetic field of $H = 5$ T was applied along the axis c. The flipping ratios for over 110 (hkl) observed reflections with $l = 0,1,2,3,4$ have been measured at $T = 5$ K.

C. XMD

In the joint refinement and MEM reconstructions we used the data from the XMD experiment performed earlier on the BL3C3 beamline of the Photon Factory of KEK in Tsukuba, Japan [10,13]. These measurements were made at 15 K with a magnetic field of 0.85 T, which is sufficient to saturate the magnetization along any axis in the bc plane [19]. The flipping ratios were measured for 47 independent reflections:

$$R_{\text{XMD}} = \frac{I_+ - I_-}{I_+ + I_-} = \gamma f_P \frac{F_{\text{MS}}}{F_{\text{ch}}} \sin\theta. \quad (2)$$

Here I_+ and I_- are the scattering intensity before and after the magnetization reversal, γ is the energy factor given as $\gamma = \hbar\omega/mc^2$ where $\hbar\omega$ is the energy of x rays and mc^2 is the electron rest mass energy, f_P is the polarization factor, F_{MS} and F_{ch} are the spin part of magnetic structure factor and the charge structure factor, respectively, and θ is the Bragg angle set to $45°$ for that experiment.

It should be noted that the $Pbnm$ space group, equivalent to $Pnma$, was used for the description of YTiO$_3$ crystal structure in Refs. [10,13]. In the present paper the standard $Pnma$ space group is used.

III. RESULTS

A. Nuclear structure and extinction

The integrated intensities measured on 5C2 at 40 and 300 K were used for the structural refinement in the $Pnma$ space group. The refinement process includes the atomic positions and isotropic temperature parameters plus six additional extinction parameters according to an anisotropic extinction model implemented in FULLPROF [20]. The extinction is described by the y_{hkl} coefficient which gives a relation between the experimentally measured intensity of Bragg reflection, I_{exp}, and the intensity I_0, "corrected" for extinction:

$$I_{\text{exp}} = y_{hkl} I_0. \quad (3)$$

This coefficient is expressed as a scalar function of the extinction parameter q_{hkl}, the wavelength λ, the structure factor F_{hkl}, and the diffraction angle 2θ:

$$y_{hkl} = \frac{1}{\sqrt{1 + 2.5 \times 10^{-4}\left(\frac{q_{hkl} F_{hkl}^2 \lambda^3}{\sin 2\theta}\right)}}, \quad (4)$$

TABLE I. Structure parameters of YTiO$_3$ at 40 K from structural refinement on 280 unique reflections with obtained agreement R factor of 0.03.

Atom	x	y	z	B_{iso} (Å^2)
Y	0.0739(1)	0.25	0.9780(1)	0.24(1)
Ti	0.5	0	0	0.17(2)
O$_1$	0.4577(1)	0.25	0.12081(7)	0.28(1)
O$_2$	0.3093(1)	0.05801(5)	0.69042(8)	0.29(1)
$a = 5.6844(31)$ Å, $b = 7.5873(44)$ Å, $c = 5.3104(47)$ Å				

with $q_{hkl} = (q_1 h^2 + q_2 k^2 + q_3 l^2 + q_4 hk + q_5 hl + q_6 kl)$ $(\lambda/\sin\theta)^2$ and $q_1,..., q_6$ as refinable parameters. An accurate description of extinction effects has crucial importance for polarized neutron-diffraction measurements because extinction has a very strong influence both on unpolarized diffraction intensity and on flipping ratio used for the determination of magnetic structure factor [Eq. (1)].

The refinement results are given in Table I for data measured at 40 K in the paramagnetic phase. The anisotropic thermal parameters are provided in Table 2S of Ref. [18]. The obtained structure parameters are in agreement with literature [12,21,22]. Data treatment without extinction correction leads to worsening the goodness of fit by a factor of 20. Extinction parameters obtained in the refinement do not show any considerable dependence on the temperature.

To exclude a possible lowering of *Pnma* symmetry due to the orbital ordering, detailed structure studies were performed on the single-crystal diffractometer TOPAZ at 90 K and room temperature. As in the 5C2 experiment, a certain number of weak reflections (about 350 at each temperature) violating *Pnma* extinction rules were found. However, detailed analysis of systematic absences and reflection conditions using the SUPERFLIP program from JANA2006 [23] confirms the *Pnma* space group as described in Ref. [18]. We believe that the observation of some systematically absent reflections in neutron diffraction is attributable to multiple scattering effects as observed in previous x-ray-diffraction experiments [12].

B. Magnetization density reconstruction

Nuclear structure factors and extinction parameters deduced from the unpolarized neutron experiments were used to derive the magnetic structure factors by solving Eq. (1).

Since the crystal structure is centrosymmetric, the magnetization density can be directly reconstructed from the measured magnetic structure factors by a model-free MEM [24]. Figure 1(a) shows the reconstructed three-dimensional magnetization density when all measured magnetic structure factors are included in the reconstruction procedure. The antiferromagnetic ordering of 3d orbitals in the YTiO$_3$ compound is clearly seen in Fig. 1(a). The lobes of the 3d orbitals become even more pronounced if the density reconstruction is performed by using only special reflections for which the contribution of the spherical part of the magnetic density of titanium into the magnetic structure factor is equal to zero [see Fig. 1(b); the number of reflections is 190]. Such a reconstruction of spin density based on special reflections measured by XMD technique was used previously [25].

We also note that the magnetization density depicted in Fig. 1(a) shows weak magnetic density contributions located near the apical oxygen O$_1$ in 4c position. Summation of the density around each atom provides a rough estimate of magnetic moments. The magnetic moment of each atom is the following: $0.743\mu_B$ for titanium, $0.035\mu_B$ for oxygen O$_1$, $0.021\mu_B$ for oxygen in general position O$_2$, and $-0.044\mu_B$ for yttrium.

C. Spin-density model refinement of PND and XMD data

In this refinement, the magnetic structure factors are calculated from the spin density, which is modeled as a superposition of the spin densities of titanium, oxygen, and yttrium atoms [26]. In the case of titanium atoms the spin density is estimated as the square of the modulus of the wave function of an unpaired electron as described in the restricted Hartree-Fock method [24]. In this method the wave function is considered as a linear combination of Slater-type atomic functions:

$$\psi = \sum_{L=0}^{N-1} R_L(n_L, \xi_L, r) \sum_{M=-L}^{L} \alpha_{LM} Y_{LM}(\theta, \phi), \qquad (5)$$

where the values N, L, and M are the quantum numbers (N is the principal quantum number, L is the azimuthal quantum number, and M is the magnetic quantum number); $R_L(n_L, \xi_L, r)$ is the Slater-type radial function; and $Y_{LM}(\theta, \phi)$ is the real spherical harmonics [26]. Coefficients α_{LM} are the
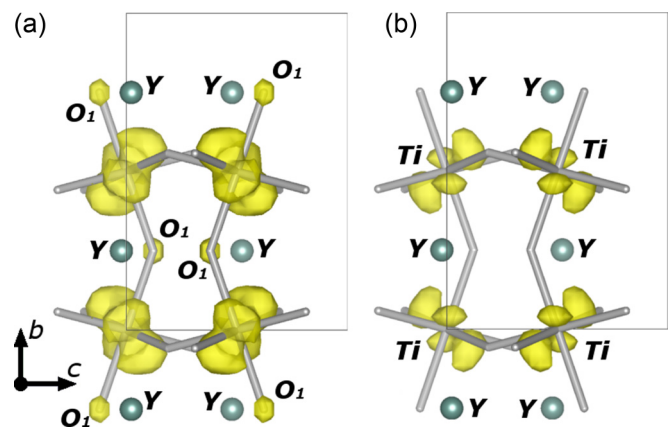

FIG. 1. Magnetization density reconstructed by maximum entropy method with (a) all measured reflections (the level of isodensity surface is 0.05 μ_B/Å^3) and (b) "special" reflections originating from the aspherical contribution of the Ti spin-density distribution (the level of isodensity surface is 0.10 μ_B/Å^3).
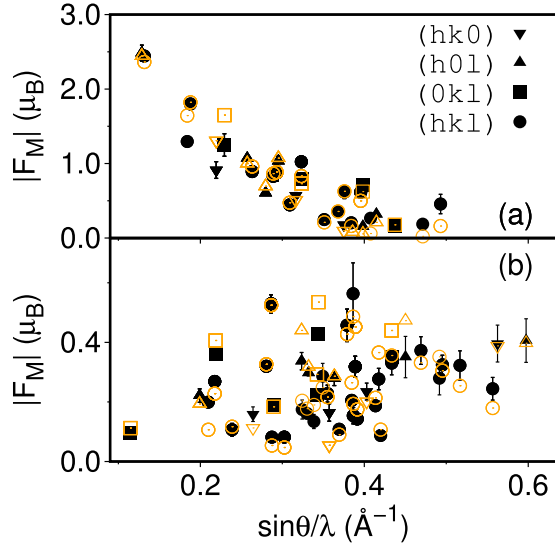
FIG. 2. Observed (filled symbols) and calculated (open symbols) modulus of magnetic structure factors as a function of $\sin\theta/\lambda$ for PND data. Only unique reflections with nonzero (a) and zero (b) contribution of the spherical part of magnetic density of titanium into magnetic structure factor are shown.

atomic orbital coefficients with the normalization condition. The wave function of an unpaired $3d$ electron of titanium Ti^{3+} has been refined with the following parameters: $N = 3$, $n_L = 2$, $\xi = 2.7$ and nonzero coefficients α_{LM} at $L = 2$ [27].

The real spherical harmonics are defined in a local Cartesian coordinate system belonging to each titanium atom (see Fig. 1S in Ref. [18]). The local axes point to neighboring oxygens. The z axis is directed towards the O_2' atom, which is farthest from titanium (2.08 Å). The x axis is directed towards the O_1 atom. The y axis has a direction towards the O_2 atom. Distances from titanium to O_1 and O_2 atoms are approximately equal to 2.02 Å.

For the description of spin density on the oxygen and yttrium atoms, the spherical model has been applied:

$$\rho_{\text{sph}}(r) = \frac{1}{4}\pi \times \mu \times R_L(n_L, \xi_L, r),\qquad(6)$$

where μ is the atomic magnetic moment. The Slater-type radial function has parameters $n_L = 2$, $\xi_L = 4.45$ for oxygen and $n_L = 6$, $\xi_L = 7.98$ for yttrium [27].

The applied procedure is more universal for refinement of experimental data than the analytical expressions used previously [6,10]. More details about the model refinement of the spin density are available in literature [24].

The PND data refinement gives good agreement between calculated and experimentally observed flipping ratios (Fig. 2). The parameters of the model are listed in Table II. The refined wave function of the unpaired electron of titanium in the asymmetric unit is

$$\psi = \sqrt{0.61(6)}\,|yz\rangle + \sqrt{0.39(3)}\,|xz\rangle,\qquad(7)$$

where $3d$ orbitals $|yz\rangle$ and $|xz\rangle$ are described by the real spherical harmonics $Y_{2-1}(\theta,\phi)$ and $Y_{2+1}(\theta,\phi)$, respectively.

We applied our refinement procedure to the experimental XMD data. The comparison between calculated and exper-

TABLE II. Atomic magnetic moments (in μ_B) and titanium $3d$ orbital populations in ferromagnetic $YTiO_3$ from orbital model refinement with PND, XMD, and joint PND-XMD data for two weighting schemes (see text).

			Joint PND-XMD	
	PND	XMD	Scheme 1	Scheme 2
Ti (μ_B)	0.715(4)	0.597(47)	0.713(4)	0.708(5)
$P(xy)$	0.0	0.0	0.0	0.0
$P(xz)$	0.39(3)	0.53(4)	0.44(2)	0.47(2)
$P(yz)$	0.61(6)	0.43(6)	0.55(4)	0.51(4)
$P(z^2)$	0.001(1)	0.03(1)	0.010(3)	0.022(4)
$P(x^2 - y^2)$	0.0005(7)	0.003(3)	0.0000(1)	0.0000(1)
O_1 (μ_B)	0.016(4)	0.05(4)	0.013(4)	0.009(5)
O_2 (μ_B)	0.004(3)	$-0.08(4)$	0.005(3)	0.005(4)
Y (μ_B)	$-0.047(4)$	$-0.14(4)$	$-0.049(4)$	$-0.053(5)$
N_{obs}	286	62	348	348
GOF	5.3	3.5	5.4	5.6

imentally measured magnetic structure factors is shown in Fig. 3. Similar parameters of the model have been obtained (column 3 in Table II).

In spite of a smaller number of reflections in the case of the XMD experiment compared to the PND one (62 points against 286 points), the refinement gives a similar distribution of the unpaired $3d$ electron of titanium and thus comparable information about the antiferromagnetic orbital ordering phenomenon. The error bars of magnetic moments of atoms are high because of the absence of reflections with low momentum transfer. The XMD data are restricted to the high momentum transfer reflections ($\sin\theta/\lambda > 0.3$ Å), for which a magnetic scattering is highly reduced due to the decrease of magnetic form factor versus resolution. For the same reason, introducing magnetic moments on oxygen and yttrium atoms does not significantly improve refinement of XMD data.

For the joint refinement of magnetic structure factors two weighting schemes were used. The first scheme minimizes the sum of the goodness of fit of each experiment [16,28,29]. This weight usually favors the experiment that provides a large data set. The refinement results performed by the scheme are presented in column 4 of Table II.
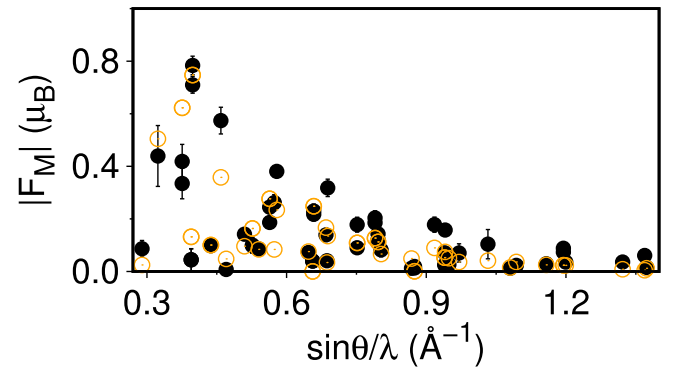

FIG. 3. Observed (filled symbols) and calculated (open symbols) modulus of magnetic structure factors as a function of $\sin\theta/\lambda$ for XMD data.

TABLE III. Theoretical atomic spin populations in $YTiO_3$ in the framework of the Bader model (in $e-$) and Ti $3d$-orbital populations (normalized to 1).

Bader spin population		$3d$-orbital population of the Ti atom	
Ti	0.852	$P(xy)$	0.0
O_1	0.036	$P(xz)$	0.46(1)
O_2	0.049	$P(yz)$	0.54(2)
Y	0.015	$P(z^2)$	0.002(1)
		$P(x^2 - y^2)$	0.0000(1)

The second weighting scheme is based on the minimization of the sum of the goodness of fit normalized per data number for each experimental technique. It reduces the weighting ratio between large and small data sets and hence should better take into account the contribution of the small data set. The results are given in column 5 of Table II. Both weighting schemes give the same results, not statistically different from PND only.

The population of $3d$ orbitals is in agreement with our XRD measurements performed at 100 K [22], where similar populations of $|xz\rangle$ and $|yz\rangle$ orbitals were observed. The $3d$ electron lobe orientations of the titanium atom are similar for the static deformation density calculated from XRD measurements and reconstructed spin density (Fig. 4)

In addition to the magnetic moment on the titanium atom, small magnetic moments on the oxygen O_1 and yttrium atom are observed. It should be noted that the presence of small magnetization on oxygen and yttrium may be related to our recent XRD measurements, where anisotropic accumulation of electrons around these atoms was observed [22].

D. DFT computations

Ab initio computations based on density functional theory were done for $YTiO_3$ to compare with experiment. The computations were performed by the CRYSTAL14 package [30], which is optimized for periodic calculations. The calculations were carried out at the density functional theory level, using the PBE0-1/3 [31] hybrid functional and optimized basis set proposed in Refs. [32,33]. One unpaired electron per Ti atom was attributed as an initial guess. The theoretical spin populations obtained by Bader analysis performed by the TOPOND package [34] are presented in Table III. The theoretical $3d$ orbital populations reported in Table III were estimated by applying the previously defined orbital model refinement to the calculated magnetic structure factors. The calculated spin density in the Ti-O_1-O_2' plane is displayed in Fig. 5 for comparison with the results of the model refinement on experimental data [Fig. 4(a)].

The population of $3d$ orbitals of the titanium atom is well consistent with the experimental results (see Tables II and III). The lobes of the $3d$ orbitals as shown by Figs. 4(a) and 5 demonstrate identical orientation for experiment and theory.

Besides the spin population on the titanium atom, the Bader analysis shows a small population on oxygen and yttrium atoms. The estimated spin population on the oxygen O_1 atom (4.1% relative to the population on titanium) is in agreement with experimental magnetic moment 0.013(4) μ_B, which is
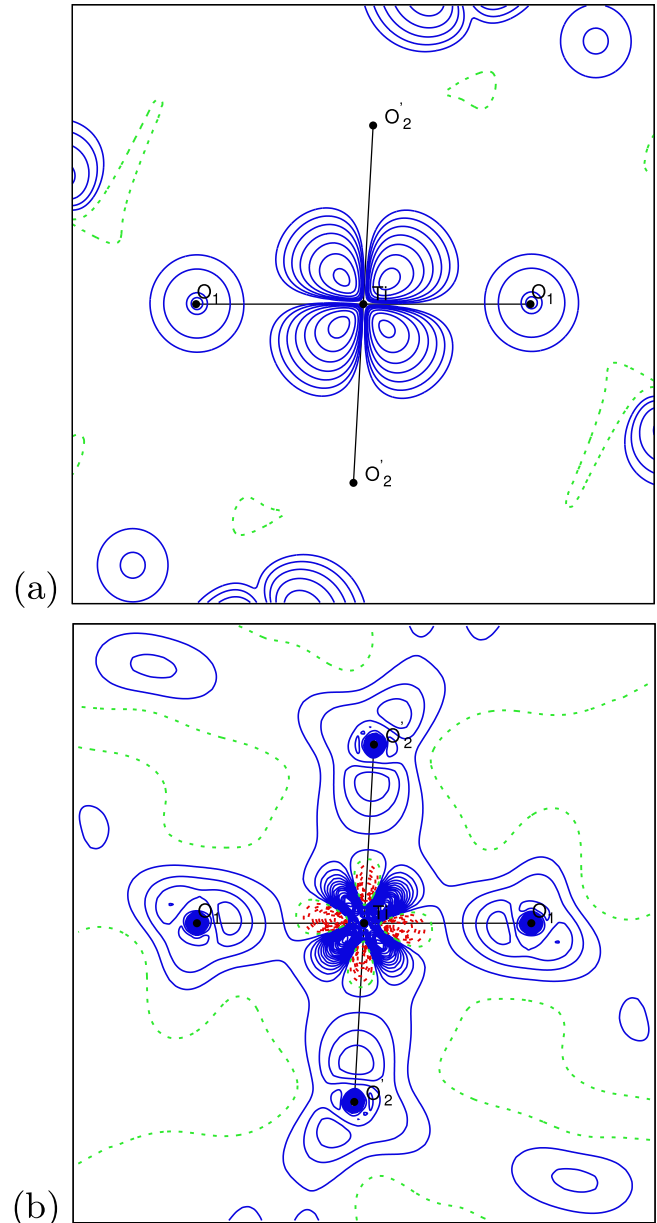

(a)

(b)

FIG. 4. (a) Experimental spin density from joint PND-XMD model refinement (normalized to 1 per TiO_6 unit) in the Ti-O_1-O_2' plane. Contours at intervals of 0.01×2^n ($n = 0, \ldots, 12) \mu_B$ Å^{-3}: positive, blue lines; negative, red dashed lines; and neutral, green dashed lines. (b) Static deformation density from x-ray diffraction at 100 K [22]. Contours at intervals of $0.1 e$ Å^{-3}: positive, blue lines; negative, red dashed lines; and neutral, green dashed lines.

1.8(6)% relative to the titanium magnetic moment as obtained by PND-XMD joint refinement in scheme 1 (Table II).

The DFT calculations show a nonzero spin population on oxygen O_2, even larger than the O_1 population. However, no significant magnetic moment on O_2 atoms was observed from refinement of experimental data. The spin population on the O_2 atom given by DFT calculation looks overestimated [35,36].

The small magnetic moment observed on oxygen O_1 in the $YTiO_3$ compound may be significant for the understanding the role of this atom in mediating magnetic interactions between
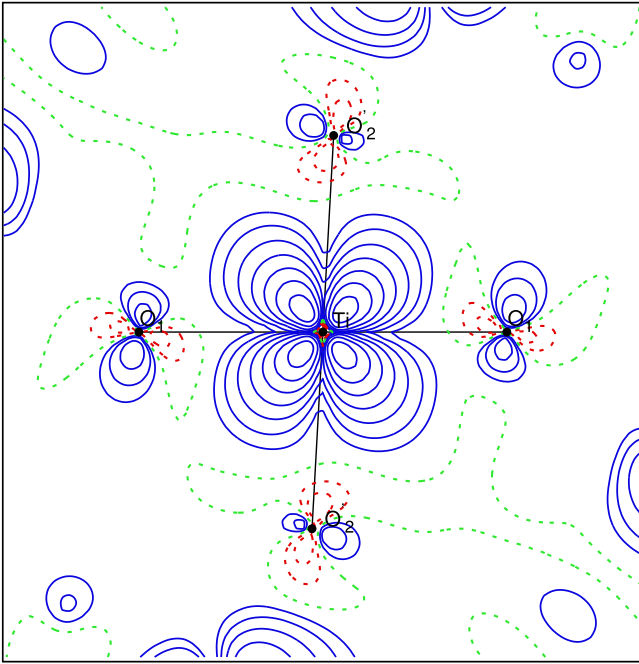
FIG. 5. Spin density in the Ti-O_1-O_2' plane calculated by DFT. Contours at intervals of 0.01×2^n ($n = 0, \ldots, 12$)μ_B Å^{-3}: positive, blue lines; negative, red dashed lines; and neutral, green dashed lines.

neighboring Ti coordination polyhedra. It is widely recognized that the magnetic interaction between the neighboring Ti t_{2g} orbitals is governed by the superexchange processes mediated by the O $2p$ orbitals [1]. At these orbitals the t_{2g} bandwidth is reducing with decreasing the Ti-O-Ti bond angle. Because the bond angle for the O_1 atom is smaller than for the O_2 atom—140.3 versus 143.7°—the magnetic exchange between titanium atoms is expected to occur mainly through the O_1 atom. The negative spin density located on the yttrium atom could result from spin polarization due to the positive spin density on the O_1 atom of the two short Y-O_1 bonds (2.23 and 2.31 Å) of the Y surrounding.

It should be noted that DFT calculations do not evidence any spin population on the yttrium atom, contrary to the PND data analysis, which exhibits a negative spin population on this atom. Indeed DFT calculations generally provide a qualitative agreement with experimental spin densities from PND but do not allow one to describe very fine details of the spin distribution, which requires a higher level of theory like the complete active space self-consistent field (CASSCF) method [37]. A recent paper [38] confirms that, in the case of a multireference system which corresponds to a single d electron that could occupy any d orbital, the CASSCF approach is proved to give better results than DFT.

IV. CONCLUSION

The model free reconstruction by the maximum entropy method of the magnetization density in the ferromagnetic $YTiO_3$ based on PND measurements provides direct observation of orbital ordering of $3d$ orbitals of titanium and observation of a magnetic moment on the oxygen atoms in $4c$ position of the $Pnma$ space group. The joint model refinement of PND and XMD data shows that the titanium $3d$ electron wave function can be described by a combination of $|xz\rangle$ and $|yz\rangle$ orbitals. The positive spin population obtained on the O_1 atom is in agreement with DFT calculations and recent results of charge density studies [22]. The PND-XMD joint refinement method opens the way to accurate spin-density determination in transition-metal compounds presenting an orbital contribution to the magnetization density.

[1] M. Mochizuki and M. Imada, New J. Phys. **6**, 154 (2004).

[2] H. Sawada and K. Terakura, Phys. Rev. B **58**, 6831 (1998).

[3] J. Choukroun, Phys. Rev. B **84**, 014415 (2011).

[4] M. Itoh and M. Tsuchiya, J. Magn. Magn. Mater. **226**, 874 (2001).

[5] C. Ulrich, G. Khaliullin, S. Okamoto, M. Reehuis, A. Ivanov, H. He, Y. Taguchi, Y. Tokura, and B. Keimer, Phys. Rev. Lett. **89**, 167202 (2002).

[6] J. Akimitsu, H. Ichikawa, N. Eguchi, T. Miyano, M. Nishi, and K. Kakurai, J. Phys. Soc. Jpn. **70**, 3475 (2001).

[7] B. Li, D. Louca, B. Hu, J. L. Niedziela, J. Zhou, and J. B. Goodenough, J. Phys. Soc. Jpn. **83**, 084601 (2014).

[8] H. Nakao, Y. Wakabayashi, T. Kiyama, Y. Murakami, M. V. Zimmermann, J. P. Hill, D. Gibbs, S. Ishihara, Y. Taguchi, and Y. Tokura, Phys. Rev. B **66**, 184419 (2002).

[9] F. Iga, M. Tsubota, M. Sawada, H. B. Huang, S. Kura, M. Takemura, K. Yaji, M. Nagira, A. Kimura, T. Jo, T. Takabatake, H. Namatame, and M. Taniguchi, Phys. Rev. Lett. **93**, 257207 (2004); **97**, 139901(E) (2006).

[10] M. Ito, N. Tuji, F. Itoh, H. Adachi, E. Arakawa, K. Namikawa, H. Nakao, Y. Murakami, Y. Taguchi, and Y. Tokura, J. Phys. Chem. Solids **65**, 1993 (2004).

[11] N. Tsuji, M. Ito, H. Sakurai, K. Suzuki, K. Tanaka, K. Kitani, H. Adachi, H. Kawata, A. Koizumi, H. Nakao, Y. Murakami, Y. Taguchi, and Y. Tokura, J. Phys. Soc. Jpn. **77**, 023705 (2008).

[12] J. R. Hester, K. Tomimoto, H. Noma, F. P. Okamura, and J. Akimitsu, Acta Cryst. **B53**, 739 (1997).

[13] S. Tsuji, Master's thesis, Gunma University, 2004; H. Akiyama, Master's thesis, Gunma University, 2006.

[14] A. Gukasov, S. Rodrigues, J.-L. Meuriot, T. Robillard, A. Sazonov, B. Gillon, A. Laverdunt, F. Prunes, and F. Coneggo, Phys. Procedia **42**, 150 (2013).

[15] A. Gukasov, A. Goujon, J.-L. Meuriot, C. Person, G. Exil, and G. Koskas, Physica B **397**, 131 (2007).

[16] M. Deutsch, B. Gillon, N. Claiser, J.-M. Gillet, C. Lecomte, and M. Souhassou, IUCrJ **1**, 194 (2014).

[17] Z. Yan, I. A. Kibalin, N. Claiser, S. Gueddida, B. Gillon, A. Gukasov, A. B. Voufack, F. Morini, Y. Sakurai, M. Brancewicz, M. Itou, M. Itoh, N. Tsuji, M. Ito, M. Souhassou, C. Lecomte, P. Cortona, and J.-M. Gillet, Phys. Rev. B **96**, 054427 (2017).

[18] See Supplemental Material at http://link.aps.org/supplemental/10.1103/PhysRevB.96.054426 for details on data collection, refined structural parameters, crystal structures solution of $YTiO_3$, and definition of the local coordinate system for different sites of titanium atoms.

[19] N. N. Kovaleva, A. V. Boris, P. Yordanov, A. Maljuk, E. Brückner, J. Strempfer, M. Konuma, I. Zegkinoglou, C. Bernhard, A. M. Stoneham, and B. Keimer, Phys. Rev. B **76**, 155125 (2007).

[20] J. Rodriguez-Carvajal, Physica B **192**, 55 (1993).

[21] A. C. Komarek, H. Roth, M. Cwik, W.-D. Stein, J. Baier, M. Kriener, F. Bouree, T. Lorenz, and M. Braden, Phys. Rev. B **75**, 224402 (2007).

[22] A. B. Voufack *et al.*, 2017 (private communication).

[23] L. Palatinus and G. Chapuis, J. Appl. Cryst. **40**, 786 (2007).

[24] B. Gillon and P. Becker, Magnetization densities in material science, in *Modern Charge Density Analysis*, edited by C. Gatti and P. Macchi (Springer, Dordrecht, 2012).

[25] K. Suzuki, M. Ito, N. Tsuji, H. Adachi, H. Nakao, Y. Murakami, Y. Taguchi, Y. Tokura, E. Nishibori, and M. Sakata, Photon Factory Activity Report 2007 **25B**, 83 (2008).

[26] N. Hansen and P. Coppens, Acta Crystallogr. **A34**, 909 (1978).

[27] E. Clementi and C. Roetti, At. Data Nucl. Data Tables **14**, 177 (1974).

[28] M. Deutsch, N. Claiser, S. Pillet, Y. Chumakov, P. Becker, J.-M. Gillet, B. Gillon, C. Lecomte, and M. Souhassou, Acta Cryst. **A68**, 675 (2012).

[29] J. A. K. Duckworth, B. T. M. Willis, and G. S. Pawley, Acta Cryst. **A25**, 482 (1969).

[30] C. Pisani, *Quantum-Mechanical Ab-Initio Calculation of the Properties of Crystalline Materials* (Springer, Berlin, 1996).

[31] C. A. Guido, E. Bremond, C. Adamo, and P. Cortona, J. Chem. Phys. **138**, 021104 (2013).

[32] A. Buljan, P. Alemany, and E. Ruiz, J. Phys. Chem. B **103**, 8060 (1999).

[33] A. Erba, K. E. El-Kelany, M. Ferrero, I. Baraille, and M. Rérat, Phys. Rev. B **88**, 035102 (2013).

[34] C. Gatti, V. R. Saunders, and C. Roetti, J. Phys. Chem. **101**, 10686 (1994).

[35] K. Boguslawski, C. R. Jacob, and M. Reiher, J. Chem. Theory Comput. **7**, 2740 (2011).

[36] C. R. Jacob and M. Reiher, Int. J. Quantum Chem. **112**, 3661 (2012).

[37] A. B. Voufack, N. Claiser, C. Lecomte, S. Pillet, Y. Pontillon, B. Gillon, Z. Yan, J.-M. Gillet, M. Marazzi, A. Genoni, and M. Souhassou, Acta Cryst. **B73**, 544 (2017).

[38] P. Verma and D. G. Truhlar, Phys. Chem. Chem. Phys. **19**, 12898 (2017).